A multivariate investigation of bio-inspired geometries on rocket fins in subsonic and supersonic flow

Makam I

Submitted: July 18, 2025, Revised: version 1, August 29, 2025
Accepted: September 2, 2025

Abstract
The aerodynamic efficiency of a rocket is significantly influenced by its fin design. This study explored the use of bio-inspired fin geometries on shark skin riblets and humpback whale tubercles to reduce drag on a model rocket in both subsonic (30 m/s) and supersonic (Mach 1) flow regimes using Computational Fluid Dynamics (CFD). Simulations in ANSYS Fluent were performed for a conventional smooth fin (baseline) and for fins with riblet and tubercle modifications. The bio-inspired designs altered the boundary layer on the fin surfaces, affecting flow separation and pressure distribution. Key results indicated that whale-inspired tubercle fins consistently lowered drag in both speed regimes by up to 11%, by delaying flow separation and reducing pressure drag. Shark skin riblets displayed mixed performance: they increased drag at low speed, due to higher skin friction, but achieved a 6% drag reduction at Mach 1 by mitigating form drag in the wake. These findings demonstrate the potential of nature's geometries on rocket fins to strategically leverage turbulence for drag reduction.

Keywords
Bio-inspired Aerodynamics, Computational Fluid Dynamics, Drag reduction, Tubercles, Riblets, Boundary layer, Rocket fin design, Reynolds number, Turbulent flow, Biomimicry

---

Ishaan Makam, Newport High School, 4333 Factoria Blvd. SE Bellevue, WA 98006, USA.
ishaan.makam@gmail.com

https://doi.org/10.64336/001c.144090

Introduction

Aerodynamic drag poses one of the most significant challenges in aerospace engineering. In the early stages of ascent, the rocket is likely at subsonic speed where boundary layers tend to remain laminar (1). As velocity increases, rockets enter compressible and eventually supersonic regimes, where shock waves, boundary layer separation, and turbulence create aerodynamic losses (2). Drag that is induced on the rocket primarily stems from pressure differences and base vortices (3). There are two types of aerodynamic drag: form drag and skin friction drag. Form drag, also called pressure drag, is primarily formed by pressure differences and a larger wake area which stems from increased flow separation. On the other hand, skin friction drag is formed by frictional forces between the surface and the boundary layer (4). Optimizing passive drag reduction techniques generally improves rocket efficiency.

Understanding the aerodynamic environment in which rockets operate is essential for developing effective drag reduction strategies. The Reynolds number, a dimensionless parameter that relates inertial to viscous forces, is what determines whether flow is laminar or turbulent. At low Reynolds numbers, flow tends to be laminar, while at higher values, it becomes turbulent (5). Rockets, due to their high velocities and large characteristic lengths, usually operate at extremely high Reynolds numbers, often $> 10^6$ which constitutes turbulent flow.

Nature offers time-tested strategies for passive flow control. Sharks use riblet-like grooves on their skin to organize turbulence and reduce friction drag as they swim (Figure 1). These riblets align turbulent vortices into streamwise patterns, which helps minimize crossflow and lower skin friction (6). Similarly, humpback whales use leading-edge tubercles on their flippers, which generate spanwise vortices that stabilize flow and delay separation (7). These adaptations improve control and efficiency by reducing pressure drag and preserving attached flow along the surface (Figure 2). Riblets and tubercles each serve distinct purposes: riblets streamline turbulence already present at high speeds, while tubercles generate controlled vortices that mitigate flow separation.

Bio-inspired surface features have already achieved success in engineering. Flow-altering surface textures such as riblets and tubercles align with broader trends in aerospace engineering that explore passive flow control. Prior work has investigated riblets as vortex generators (8). Riblet textures have even been implemented on underwater vehicles (UWVs) and proven to reduce drag by ~ 3% (9). Studies from NASA have shown up to 8% reductions in drag with riblet surfaces in specific flow conditions (10). Tubercles have improved wind turbine blades and aircraft wings by delaying stall and promoting smoother lift curves (11). However, these methods have rarely been tested in applications such as rocket fins.

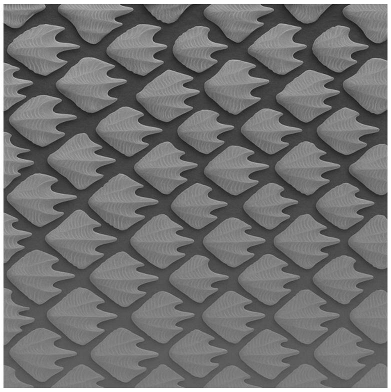

Figure 1. Shark skin riblets aligned spanwise with micro-grooves to organize turbulence. The shark skin motivated the riblet fin design.

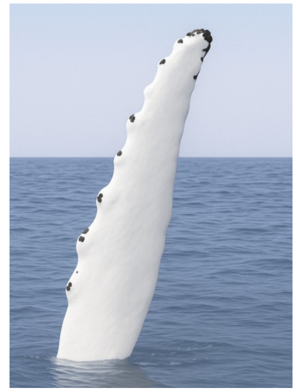

Figure 2. Humpback whale flipper with leading-edge tubercles. The sinusoidal bumps generate Vortices that delay separation, motivating the tubercled fin design.

This study investigated whether bio-inspired fin structures could improve performance in rocket-relevant conditions. Using Autodesk Fusion 360 for modeling and ANSYS Fluent for simulation, we evaluated fins with riblets and tubercles in both subsonic and supersonic regimes. A velocity of 30 m/s was selected to represent early-stage rocket flight where low-altitude speeds are under 50 m/s, producing Reynolds numbers in the transitional regime (10^5). A velocity of 343 m/s was selected to represent Mach 1 or supersonic. Our goal was to observe how these geometries affected drag, flow coherence, and turbulence using tools such as velocity pathlines, particle tracing, and Turbulent Kinetic Energy (TKE) visualizations. Although ANSYS Fluent is commercial software, the ANSYS Student edition is freely available and was used to ensure accessibility and reproducibility.

Laminar flow, which describes fluid moving in orderly, parallel layers, is typically desired because it offers lower resistance and reduces energy loss. However, in supersonic conditions, laminar flow becomes nearly impossible to maintain due to inherent instabilities in the boundary layer and the presence of strong shock waves (12). Under these conditions, turbulence forms naturally. Turbulent boundary layers possess higher momentum near the wall, enabling the flow to better resist separation by clinging to the surface and reducing wake size, in turn, reducing form drag (2).

Shark skin riblets have been found to reduce skin friction drag by organizing turbulence, but only when that turbulence already exists. At subsonic speeds, however, applying riblets may inadvertently induce turbulence by creating surface resistance. Riblets, in contrast, are designed to work within turbulent flows that are already developed to reduce flow separation. Rather than generating new vortices, they manipulate existing turbulence by guiding vortices into aligned, streamwise channels (13). These grooves reduce crossflow mixing and help maintain boundary layer attachment at high Reynolds numbers by lifting chaotic eddies away from the surface.

This difference is critical in our hypothesis. We propose that riblets will be more effective in supersonic regimes where turbulence is already present, whereas they may be detrimental at subsonic speeds (14). Tubercles, conversely, operate differently by controlling flow separation through the creation of streamwise vortices and are therefore hypothesized to perform well across both regimes. Ultimately, this work contributes to the growing intersection of biomimicry and advanced aerodynamic engineering.

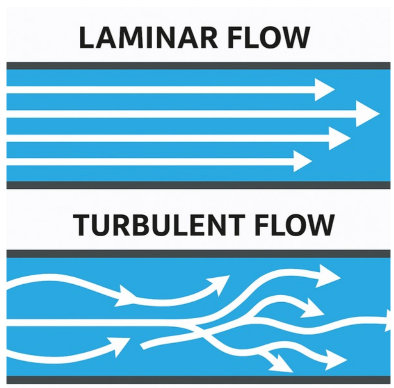

Figure 3. Conceptual diagram of laminar flow and turbulent flow boundary layers.

Literature review

Although biomimetic designs such as tubercles and riblets have been explored in other aerodynamic contexts, most notably in airfoils and turbines, their application to rocket fins remains largely unexplored. A notable exception is a dissertation by Brocksmith (2020), which evaluated the aerodynamic performance of tubercled rocket fins at high Reynolds numbers in supersonic flow (15). While Brocksmith's work offers preliminary insight into the potential benefits of tubercle modifications in hypersonic regimes, it does not address how these geometries perform under subsonic conditions or in comparison to other surface textures such as riblets. To our knowledge, this study is the first to directly compare riblet- and tubercle-inspired fin geometries on model rockets using Computational Fluid Dynamics (CFD) across both subsonic (30 m/s) and supersonic (Mach 1) conditions. It is also the first to integrate quantitative drag data with pathline visualization and turbulence diagnostics to explain flow behavior. By applying bio-inspired designs to a novel aerospace context and analyzing performance across contrasting regimes, this work offers new insights into the aerodynamic potential and limitations of surface morphologies traditionally studied outside of rocketry.

Materials and Methods

Geometry

A three-dimensional model of a rocket with four fins was created, with three fin configurations: a smooth baseline fin (no modifications), a riblet fin, and a tubercle fin. The entire rocket body was consistent between all three configurations. Figure 4 shows a diagrammatic representation of those parameters. Table 1 shows the rocket geometry and simulation parameters.

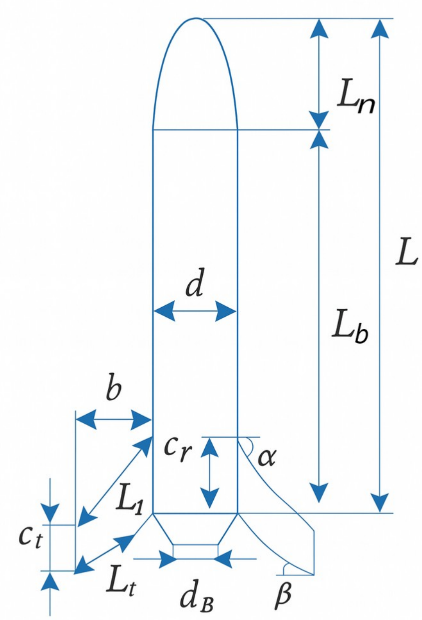

Figure 4. Labeled diagram of the model rocket showing the geometric parameters from Table 1.

Table 1. Model rocket geometry and simulation parameters

Symbol	**Description**	**Value**
α (°)	Fin leading edge sweep angle	50°
β (°)	Fin trailing edge angle	15°
b (m)	Span of the fin	0.0385673
c_r (m)	Root fin chord length	0.038
c_t (m)	Tip fin chord length	0.01
d (m)	Body tube diameter	0.0217

d_b (m)	Base diameter	0.0164
L (m)	Total length of nose and body	0.2365
L_b (m)	Length of body tube	0.165
L_l (m)	Length of leading edge of fin	0.06
L_n (m)	Nose cone length	0.0715
L_t (m)	Length of trailing edge of fin	0.033
n	Number of fins	4
S (m^2)	Reference area per fin	0.0010472
t (m)	Fin thickness	0.0007
U (m/s)	Freestream velocity	30/343
ρ (kg/m^3)	Air density	1.225
μ (kg/m·s)	Dynamic viscosity of air	0.000017894

The baseline fin has a conventional planar surface. For the riblet configuration in Figure 5, a dense array of V-shaped grooves (riblets) was applied spanwise along the fin surface to mimic shark denticles. The tubercle configuration in Figure 6 featured sinusoidal bumps along the leading edge of the fin, analogous to a humpback whale's flipper. The overall rocket and fin dimensions were kept constant across configurations. This geometric setup follows the Estes Firestreak SST model rocket as depicted in Figure 4 (16).

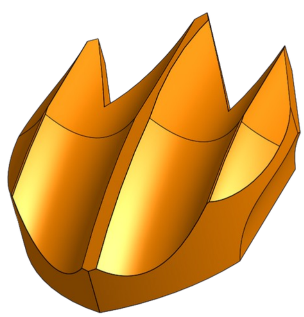

Figure 5. CAD rendering of a representative riblet unit cell showing V-shaped grooves.

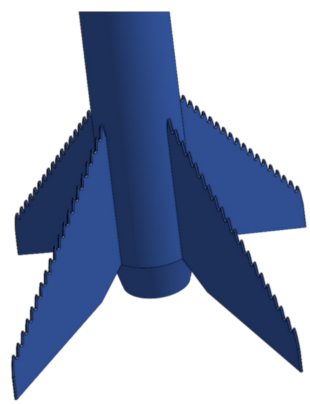

Figure 6. CAD rendering of rocket fin model featuring the sinusoidal whale tubercles on the leading edges.

Meshing

High-quality computational meshes were generated for each rocket configuration using the ANSYS Workbench suite. The meshing process began by launching the Fluid Flow (Fluent) module and dragging the created geometry to the appropriate slot under Fluid Flow. The mesh generation used a hybrid strategy: hexahedral elements were employed in the far-field region to ensure structured, efficient flow resolution with minimal numerical diffusion, while fine unstructured tetrahedral elements were used in the near-field to accurately capture the complex geometry around the rocket body and fins, including bio-inspired features like riblet grooves and tubercle curves.

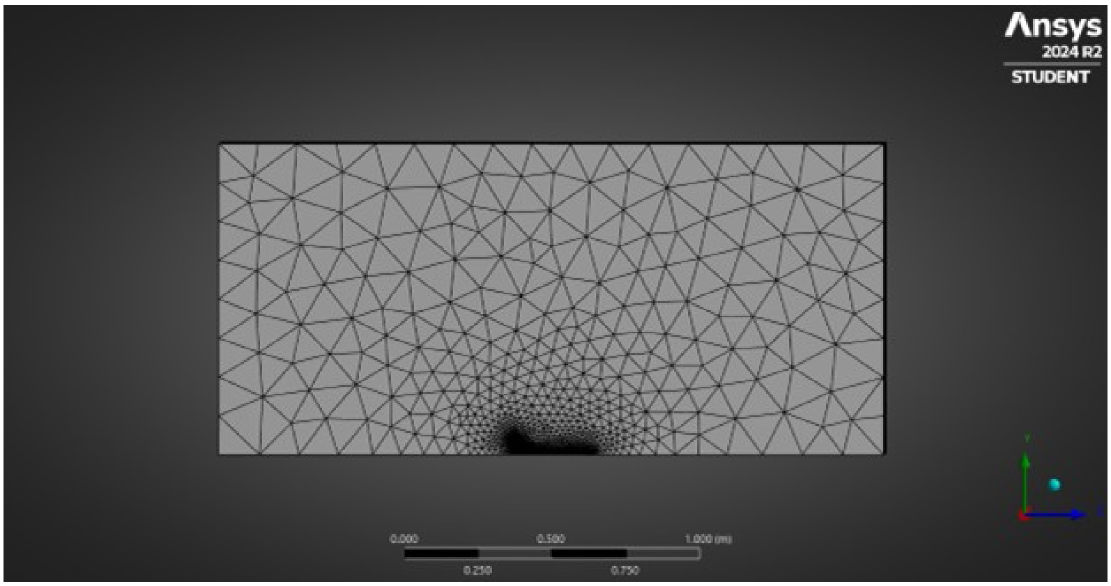

Figure 7. Computational mesh of the full rocket domain using ANSYS Fluent; fine near-wall elements and structured far-field regions are shown.

In the meshing window, proximity and curvature-based refinement settings were enabled under "Details of Mesh" to resolve intricate contours and tight clearances. Both "Capture Curvature" and "Capture Proximity" were set to "Yes," and the mesh quality was enhanced by selecting "High" smoothing. Most settings were left as default to maintain stability and consistency across different configurations, but critical values were adjusted as needed to refine performance. Local face sizing was applied specifically to the five rocket fin faces, with a minimum element size of 0.84347 mm. This value was selected to resolve the surface textures without excessive refinement that would burden solver time. The remaining geometry, including the body and enclosure, used slightly coarser sizing based on body of influence definitions.

Named selections were created for all boundary faces to facilitate physics setup in Fluent. These included velocity-inlet, pressure-outlet, symmetry planes, and the finned rocket body. The geometry was enclosed within a rectangular computational domain created with DesignModeler. This enclosure was added manually and sized to extend 0.6375 m vertically and 0.1275 m horizontally from the rocket body in all directions. These specific values ensured that flow would fully develop around the rocket without artificial confinement effects that could skew results.

Mesh refinement was concentrated around regions of high expected flow gradients, including leading and trailing edges of the fins, surface textures, and the rocket base. These areas are known to produce separation, wakes, and vortex formation, making them critical for aerodynamic evaluation. Mesh quality metrics were continuously monitored. The skewness metric, which quantifies cell shape distortion, was maintained below 0.9 to avoid numerical instability. Final meshes contained several million elements, depending on the configuration, with dense clustering around flow-critical surfaces and moderate spacing elsewhere.

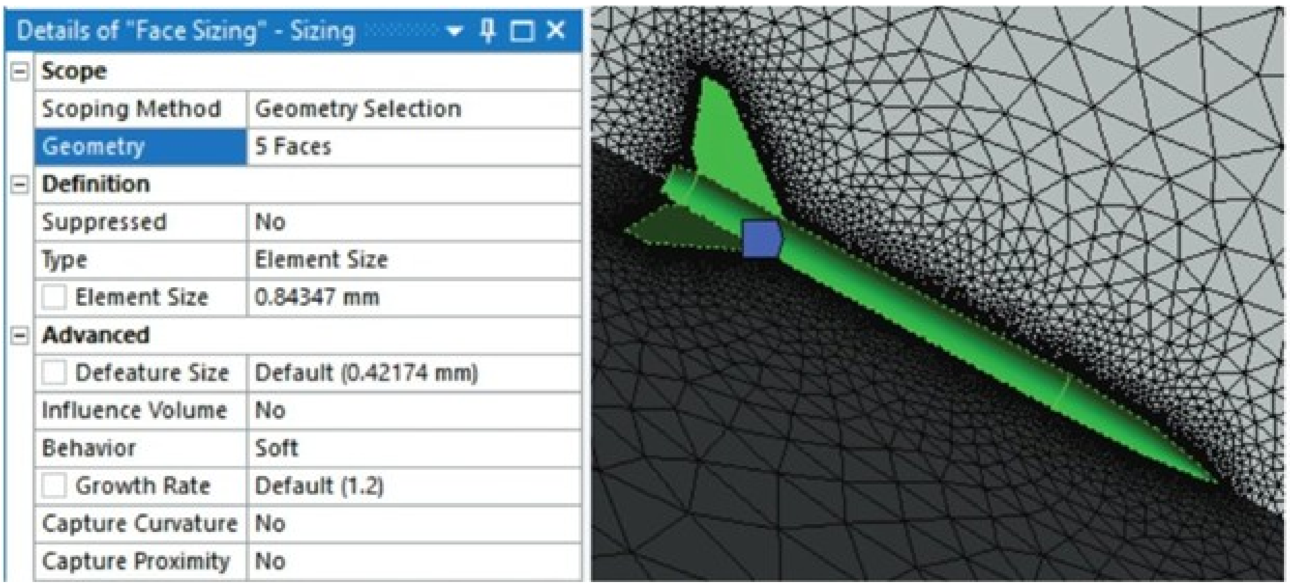

Figure 8. Meshing setup interface showing local face sizing parameters for the fins; minimum element size was set to 0.84347 mm.

Boundary conditions

Simulations were run for two freestream velocities representing different flight regimes. For the subsonic case, a velocity inlet of 30 m/s (Reynolds number on the order of 1×10^5 based on fin chord) was applied, corresponding to a low-speed launch or early flight condition. For the supersonic case, a Mach 1 inflow (343 m/s at 1 atm, sea-level conditions) was set to model transonic/supersonic cruise. In both cases, the flow was aligned with the rocket's axis (0° angle of attack). Pressure-outlet boundary conditions (0 Pa gauge) were used at the downstream boundaries to allow flow expansion. Air was modeled as an ideal gas for the Mach 1 case to capture compressibility, and as incompressible (constant density) for the 30 m/s case (since Mach ≈ 0.1).

Solver settings

The SST k–ω turbulence model was employed for all runs, as it is well-suited for capturing near-wall effects and flow separation on aerodynamic surfaces. Second-order discretization schemes were used for both momentum and pressure to improve accuracy, coupled with a pseudo-transient approach to enhance stability and convergence. Convergence criteria were stringent: all residuals had to be less than 1×10^{-6}. Convergence meant that no further iterations would change the results; in other words, the simulation reached a consistent solution. Simulations were iterated until drag forces stabilized and full convergence was achieved. For most cases, this required between 300 and 500 iterations for steady-state solutions, though some cases (especially tubercles at Mach 1) required up to 800.

To simulate flight conditions, velocity inlets were assigned –30 m/s and –343 m/s in the Z-direction (aligned with the rocket axis), corresponding to subsonic and supersonic inflows, respectively. These values matched realistic conditions for low-speed launch and Mach 1 cruise. Each configuration was simulated a minimum of ten times to ensure reproducibility. The results were then averaged to improve reliability. To quantify variability and ensure statistical robustness, each simulation was repeated ten times ($n = 10$), and the mean, standard deviation (SD), and 95% confidence intervals (CI) were calculated for all drag coefficients. Reported values are presented as mean ± CI to reflect uncertainty due to numerical and mesh discretization variability.

For the Mach 1 simulations, additional techniques were employed to assist convergence due to the presence of shocks and compressibility effects. These included relaxation factors (e.g., momentum = 0.25, turbulence = 0.75) and smaller pseudo-time steps, which helped the model converge faster. All simulations were run using ANSYS Fluent 2024 Student on a Microsoft Surface Laptop 3 equipped with an Intel® Core™ i5-1035G1 processor (4 cores, 8 logical threads, base speed 1.19 GHz, turbo up to 3.6 GHz. Mesh generation took approximately 3 hours per configuration, with an additional 2 hours per simulation for post-processing and flow visualization. All simulations were repeated ten times to ensure consistency, and reported values represent averaged results across these runs.

Data analysis

Drag force on the fins was calculated by integrating pressure and viscous forces on all fin surfaces. Surface pressure is denoted by p (in the integral), τ_w is the wall shear stress (viscous force per unit area), and n_x is the x-component of the surface normal vector (aligned with the freestream direction). The integral form allows us to separately evaluate pressure and viscous contributions to drag, which is essential for understanding how riblets and tubercles influence each mechanism. All pressure and shear data were extracted from ANSYS Fluent force reports on the fin surface.

$$C_d = \frac{2 * F_d}{\rho * v^2 * A} \rightarrow C_d = \frac{2}{\rho * v^2 * A} \int_A (p * n_x + \tau_w) dA \qquad \text{(eq1)}$$

The coefficient of drag, where *p* is freestream air density, *v* is freestream velocity, and *A* is a reference area (the platform area of one fin), was used to compare aerodynamic performance across configurations. We visualized pathlines (flow streamlines colored by velocity) to discern the overall flow pattern around the rocket, as well as contour plots of TKE and velocity magnitude in planes near the fins. These visualizations helped identify regions of flow separation, recirculation, and boundary layer development.

To further characterize the boundary layer behavior, we used the displacement thickness formula

$$\delta^* = \int_0^\infty \left(1 - \frac{u(y)}{U_\infty}\right) dy \rightarrow \delta^* \sim \int_0^{\delta_{99}} \left(1 - \frac{u(y)}{U_\infty}\right) dy \qquad \text{(eq2)}$$

which quantifies the effective thickness by which the boundary layer displaces the external flow. A thinner displacement thickness, particularly with tubercle fins, indicates better flow attachment and reduced momentum deficit near the surface. Here, u(y) is the local velocity profile normal to the surface, and u_∞ is the freestream velocity. The integral is truncated at δ_{99}, the point where velocity reaches 99% of u_∞, to limit integration to the boundary layer region. Displacement thickness δ^* was chosen because it quantifies how much the boundary layer slows the external flow, making it a direct indicator of flow attachment quality. The CFD results were post-processed in ANSYS Fluent, with images extracted to illustrate key differences among the fin configurations.

Validation strategy

Although experimental wind tunnel data was not available, several measures were taken to ensure the validity of simulation results. First, grid independence testing was performed by refining the mesh (up to ~700k elements) and confirming negligible changes (<1%) in the drag coefficient. Second, residual convergence was enforced with all residuals falling below 1×10^{-6}, and drag forces were monitored until steady-state stabilization (explained in solver settings). Third, the drag coefficients reported here fall within the expected range for axisymmetric model rockets: 0.3–0.8 in subsonic flow and 3–5 at Mach 1 (17). This alignment with published benchmarks supports the physical plausibility of the results. Additionally, a subsonic CFD study on similar geometries observed a ~68% increase in C_d when Mach number increased by ~30% (18), a trend consistent with the Mach-dependent growth observed in this study. Finally, reproducibility was ensured by repeating each configuration ten times and reporting averaged values with 95% confidence intervals.

Combined with mesh independence, strict convergence, and reproducibility testing, this grounding in literature strengthens the credibility of our results.

Results

Figure 9 illustrates representative airflow pathlines around the rocket, specifically for the baseline fin configuration under subsonic conditions (30 m/s). These pathlines, colored by velocity magnitude, highlight several key aerodynamic features. The incoming flow, shown in red, accelerates along the rocket's body and curves smoothly over the fin surfaces. However, a blue recirculation zone forms immediately behind the rocket's base, indicating flow separation. This separation leads to a large wake area contributing to pressure drag. These observations provide a visual foundation for understanding how modified fin geometries can alter wake dynamics and mitigate drag.

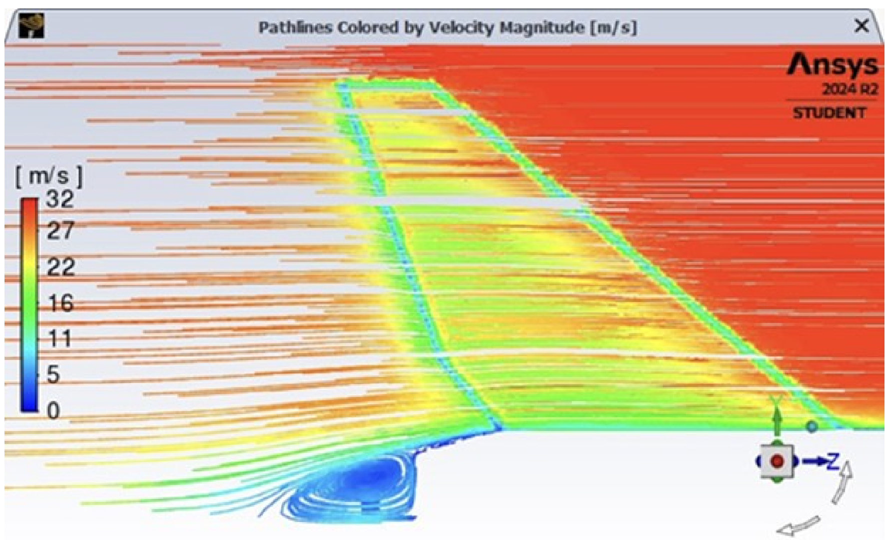

Figure 9. Velocity pathlines (colored by speed, m/s) for the baseline configuration at 30 m/s. Red indicates higher velocity; blue lower velocity. A downstream recirculation zone forms behind the base.

Table 2 quantitatively compares aerodynamic forces and drag coefficients across all three fin configurations: baseline, tubercles, and shark skin (riblets). In the subsonic regime, the baseline fin produced a drag coefficient of 0.4713 (Output by ANSYS), serving as the reference. Tubercles demonstrated a 9% drag reduction, lowering the coefficient to 0.4294 ± 0.011 (95% CI). Conversely, the shark skin configuration yielded a 60% increase to 0.7602 ± 0.022 (95% CI). In the supersonic case, tubercles reduced drag to 3.91265 ± 0.089, while riblets achieved 4.11908 ± 0.072 (Table 2). This suggests that there is a premature transition to turbulence in what would otherwise be a mostly laminar boundary layer. The riblets, while beneficial in turbulent regimes, appeared to degrade performance when applied at low Reynolds numbers where laminar flow dominates.

Table 2. Comparison of aerodynamic coefficients at subsonic and Mach 1 speeds

Coefficient Type	**Subsonic Baseline**	**Subsonic Tubercles**	**Subsonic Shark Skin**	**Mach 1 Baseline**	**Mach 1 Tubercles**	**Mach 1 Shark Skin**
Pressure Coefficient	0.12531	0.09622	0.26573	1.76212	1.37529	1.68752
Viscous Coefficient	0.34642	0.33325	0.49461	2.64049	2.53736	2.60785
Total Drag Coefficient	**0.47133**	**0.42940**	**0.76021**	**4.40261**	**3.91265**	**4.11908**

In the supersonic case (Mach 1), both biomimetic designs outperformed the baseline, highlighting the benefits of controlled turbulence at high speeds. The tubercle fins reduced the drag coefficient by 11% (from 4.40261 to 3.91265), likely due to their ability to maintain flow attachment and prevent large-scale separation in the wake. The shark skin configuration also achieved a 6% drag reduction (down to 4.11908), suggesting the riblets helped to manage turbulence. This switch compared to the subsonic case supports the idea that surface roughness elements such as riblets are better suited for turbulent, high-speed conditions. These numerical results indicate that bio-inspired riblet designs offer performance advantages, but only when aligned with the appropriate flow regime.

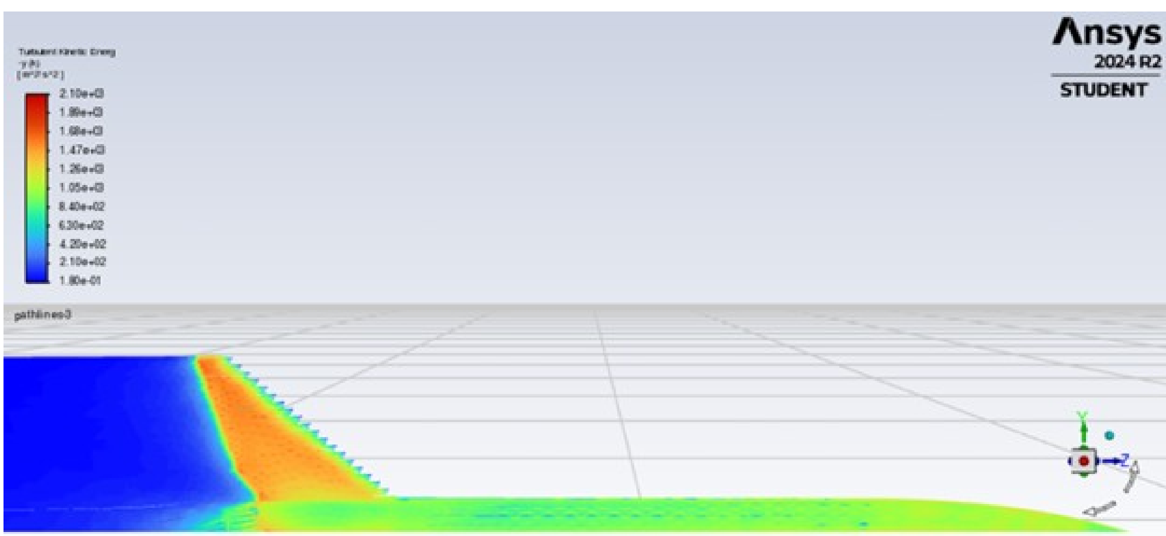

Figure 10. Turbulent kinetic energy (TKE) contours on the tubercled fin at Mach 1. Values indicate TKE magnitude from the solver; higher values appear downstream along the fin surface as vortices form over the tubercles.

To investigate these findings further, we analyzed TKE fields across the fin surface and wake. Figure 10 presents contours of the TKE for the tubercle-modified rocket at Mach 1. When the freestream flow initially impacts the fin's leading edge, TKE is low. However, as flow interacts with the sinusoidal bumps of the tubercles, vortices are generated, increasing TKE downstream (towards the rear) along the surface. This elevated turbulence stabilizes the boundary layer and suppresses large-scale separation, which is advantageous in supersonic flow. The result is better pressure recovery and reduced wake drag. However, at low speeds, this same increase in turbulence leads to higher skin friction, negating any potential benefits and even increasing total drag in some cases.

To interpret the wake dynamics behind each fin type, Figures 11 and 12 show particle pathlines colored by velocity magnitude. These visualizations illustrate both the velocity distribution and flow structure. For the baseline fin (Figure 11), the wake contains chaotic zones of low velocity, evidence of strong turbulence and early flow separation.

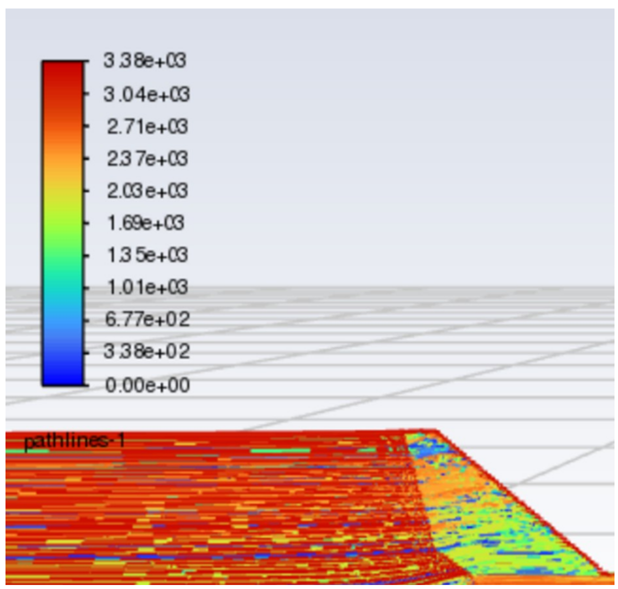

Figure 11. Velocity magnitude visualization for the baseline fin at Mach 1 with a chaotic wake and particle distribution (red color indicating higher velocity).

In contrast, Figure 12 demonstrates the organized flow structure achieved with the tubercle-modified fin design. Pathlines remained more coherent and followed defined vortex channels as they traversed the sinusoidal geometry. The induced spanwise vortices created energy in the boundary layer and prevented premature separation. This resulted in a narrower wake and more efficient momentum recovery downstream. The more organized flow in Figure 12 directly corresponds to the 11% reduction in drag coefficient seen in Table 2.

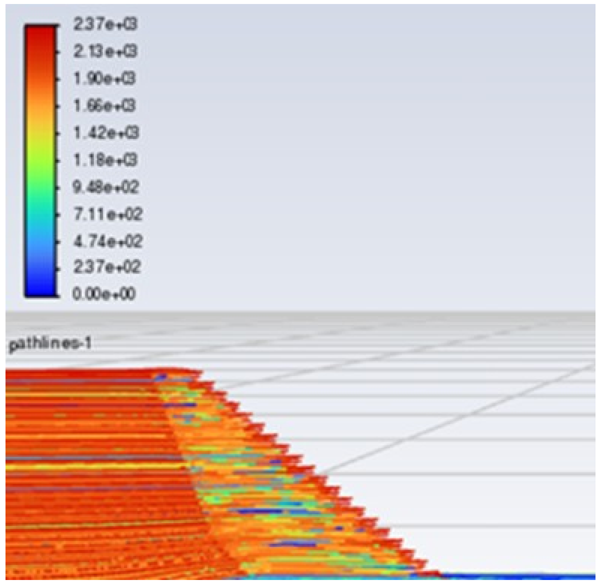

Figure 12. Velocity magnitude visualization for the tubercle fin at Mach 1 with organized vortices to reduce wake width and pressure drag.

Together, these flow visualizations, drag measurements, and TKE distributions provide a picture of how bio-inspired surface features influence aerodynamic performance. Tubercles delay separation and stabilize flow in high-speed regimes, whereas riblets show conditional benefit only when turbulence is already dominant.

Discussion

The results of this study confirm that bio-inspired fin geometries offer aerodynamic advantages under different flow regimes. Tubercles consistently reduced drag in both subsonic and supersonic conditions, whereas riblets were only effective at high speeds. This distinction has practical applications for rocket design and aerospace engineering. In launch systems where fins operate over a wide velocity range, tubercle fins may offer an improvement across both speeds by maintaining smoother pressure gradients and reducing boundary layer separation. Riblets, on the other hand, are best reserved for vehicles operating predominantly in high-speed or fully turbulent regimes, such as upper-stage rockets.

From a performance standpoint, even modest reductions in aerodynamic drag reduce costs. For example, a reduction in drag force of 11% at Mach 1, as achieved with tubercles, corresponds to a measurable decrease in the thrust required to maintain velocity. This leads to either extended range, higher payload capacity, or reduced fuel consumption. Given that launch costs can exceed $10,000 per kilogram to low-Earth orbit, even a 5% improvement in aerodynamic efficiency may yield savings in the hundreds of thousands of dollars per launch (19, 20).

This study focused exclusively on drag coefficient (C_d) because the rocket was simulated under zero angle of attack (AoA), representing vertical ascent. In such a configuration, the vehicle experiences no asymmetry in airflow and, therefore, generates negligible lift or pitching moment. Lift and moment coefficients become relevant only under off-axis flight conditions, such as angled ascent, instability, or maneuvering. Since this analysis modeled symmetric rockets in pure axial flow, those parameters were excluded. Future work may consider nonzero AoA cases to explore aerodynamic stability and control implications, especially the effect of tubercles or riblets on induced moments.

Despite these promising results, several limitations remain. CFD simulations, while powerful,
cannot fully replicate launch dynamics, such as gust loading, angle-of-attack variation, or structural vibration. Future experimental testing in wind tunnels or on subscale test vehicles will be essential to validate the drag reduction benefits observed here. Additionally, further parameter studies on riblet spacing, tubercle amplitude, and angle-of-incidence effects could uncover performance optima not explored in this study.

Conclusion

Biomimicry in rocket fin design is potentially impactful: tubercles reduced up to 11% drag in both subsonic and supersonic flow regimes, whereas shark riblets reduced drag up to 6% at supersonic flow. These results confirm that even modest geometric changes can produce meaningful aerodynamic benefits, offering a pathway toward lighter fuel demands and improved efficiency. Since this study was performed using the free ANSYS Student Edition, it remains reproducible and accessible for academic and educational use. By adapting strategies observed in nature to a new aerospace context, this work highlights how simple surface modifications can alter boundary layer behavior and wake structure in ways that are both measurable and practical. All simulation parameters and mesh details are provided to ensure transparency and reproducibility, and the findings point to future opportunities for integrating bio-inspired surfaces into rockets and other aerospace vehicles.

Acknowledgement

I would like to thank Adrian Carrillo of the University of Washington, Department of Mechanical Engineering for his mentorship and guidance throughout this project.

References

1. Benson, T. *Boundary layer*. NASA.
https://www.grc.nasa.gov/WWW/k-12/VirtualAero/BottleRocket/airplane/boundlay.html

2. Leishman, J. G. *Turbulent flows*. In *Introduction to Aerospace Flight Vehicles*. Embry-Riddle Aeronautical University.
https://eaglepubs.erau.edu/introductiontoaerospaceflightvehicles/chapter/turbulent-flows/

3. Shelton, N. *Induced drag: How it works*. Boldmethod. https://www.boldmethod.com/learn-to-fly/aerodynamics/how-induced-drag-works-with-lift/

4. Federal Aviation Administration. *Forces acting on the aircraft: Aerodynamics of flight*. FAA, 2023. https://www.faa.gov/sites/faa.gov/files/07_phak_ch5_0.pdf

5. Saldana, M., Gallegos, S., Gálvez, E., Castillo, J., Salinas-Rodríguez, E., Cerecedo-Sáenz, et al. *The Reynolds number: A journey from its origin to modern applications*. Fluids, 9(12), 2024.
https://www.mdpi.com/2311-5521/9/12/299

6. Dean, B., Bhushan, B. *Shark-skin surfaces for fluid-drag reduction in turbulent flow: A review*. Philosophical Transactions of the Royal Society A, 368(1929), 4775–4806, 2010.
https://royalsocietypublishing.org/doi/10.1098/rsta.2010.0201

7. Gopinathan, V., Bruce Ralphin Rose, J. *Aerodynamics with state-of-the-art bioinspired technology: Tubercles of humpback whale*. Proceedings of the Institution of Mechanical Engineers, Part G: Journal of Aerospace Engineering, 235(16), 2021.
https://journals.sagepub.com/doi/10.1177/09544100211001501

8. Wetzel, K., Farokhi, S. *Interaction of riblets and vortex generators on an airfoil*. AIAA Paper 1996-2428. American Institute of Aeronautics and Astronautics, 1996.
https://arc.aiaa.org/doi/10.2514/6.1996-2428

9. Kim, S., Chang, K., Lee, S.-W., Kim, M., Yoon, J., Ryu, J. *Numerical study of hydrodynamic drag effects of streamwise riblet structures on SUBOFF bare hull model*. Ocean Engineering, 310, 2024. https://doi.org/10.1016/j.oceaneng.2024.118783

10. Walsh, M. J. *Riblets for aircraft skin-friction reduction*. *Langley Symposium on Aerodynamics*, Volume 1, NASA, 1988. https://ntrs.nasa.gov/citations/19880005573

11. Ke, W., Hashem, I., Zhang, W., Zhu, B. *Influence of leading-edge tubercles on the aerodynamic performance of a horizontal-axis wind turbine: A numerical study*. Energy, 239, 2022. https://doi.org/10.1016/j.energy.2021.122186

12. ANSYS. *What is laminar flow?* ANSYS. https://www.ansys.com/simulation-topics/what-is-laminar-flow

13. Southard, J. *Introduction to fluid motions and sediment transport*. MIT OpenCourseWare, 2022.

14. Chang, P. K. *Separation of flow*. Elseiver, 2014.

15. Brocksmith, J. *Experimental and computational analysis of tubercles on rocket fins in supersonic flow*. Ph.D. dissertation, University of Alabama in Huntsville, 2019. ProQuest Dissertations Publishing.
https://www.proquest.com/openview/a32a693f023bcb592a4823b0b08ed5ee/1?cbl=18750&diss=y.

16. Cook, J. *Firestreak Rocket Estes SST*. Insane Rocketry.
https://www.insanerocketry.com/main/display/-348428751819356978/

17. Rocketry Forum. *Rule of thumb for Cd*. The Rocketry Forum, 2010. 2025.
https://www.rocketryforum.com/threads/rule-of-thumb-for-cd.39789/

18. Choudhary, S., Chakraborty, D. *Utilization of CFD for the aerodynamic analysis of a subsonic rocket*. Journal of polytechnic, 23(3), 879-887, 2020.
https://doi.org/10.2339/politeknik.711003

19. Choucair, C. *How much does it cost to launch a rocket? By type & size*. Space Insider, 2023.
https://spaceinsider.tech/2023/08/16/how-much-does-it-cost-to-launch-a-rocket/

20. Mathieu, E., Rosado, P., Roser, M. *Cost of space launches to low Earth orbit*. Our World in Data. https://ourworldindata.org/grapher/cost-space-launches-low-earth-orbit?tab=table.